Supplementary figures

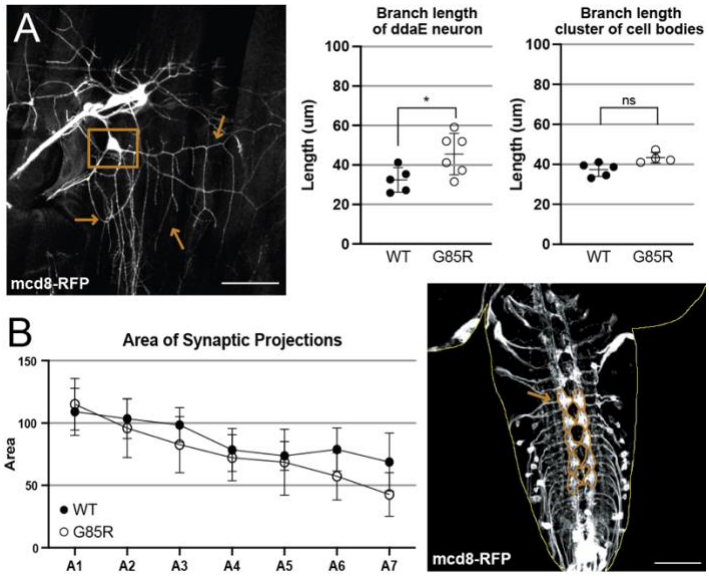

Supp 1: Area of ddaE dendrites is increased in *dSod1^{G85R}* with no change in VNC synaptic areas. **(A)** dendritic arborization in *MD>mcd8RFP* neurons, 20X mag. Unpaired t-test show a significant increase in dendritic branch length of the ddaE neuron in *dSod1^{G85R}* compared to WT. **(B)** ventral nerve cord (VNC) of *MD>mcd8RFP* neurons, 20X mag**.** Areas of *dSod1^{G85R}* synaptic regions are not significantly different from WT. Scale bar = 50um, student's t-test; (*) p-value <0.05.

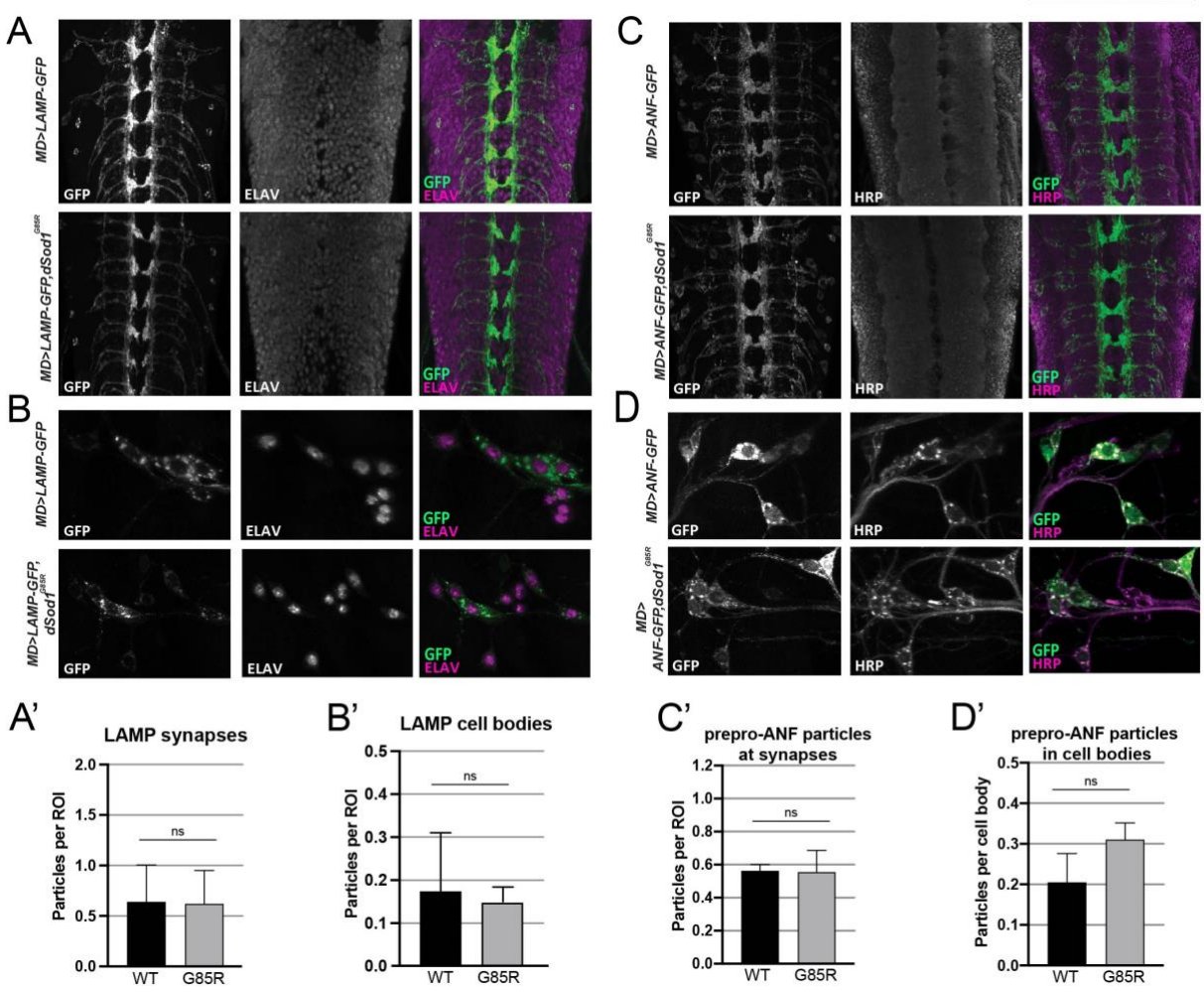

Supp 2: (A,B) LAMP1-GFP and **(C,D)** prepro-ANF-Emerald in fixed samples of synapses in midline of VNC (**A,C**) and cell bodies of MD neurons (**B,D**). (**A',B'**) Quantification of LAMP1-GFP particles in MD synapse region of VNC and cell bodies in the periphery. (**C',D'**) Quantification of prepro-ANF-Emerald particles in MD synapse region of VNC and cell bodies in the periphery. LAMP1-GFP,WT and LAMP-GFP,G85R (n=8); prepro-ANF-Emerald,WT and prepro-ANF-Emerald,G85R (n=4). (**C-F**) stained with pan-neuronal marker anti-ELAV or neuronal-membrane specific horseradish peroxidase (HRP). Quantification of fixed samples, Students' t-test; (*) p-value <0.05. Full genotypes denoted in Table 1.

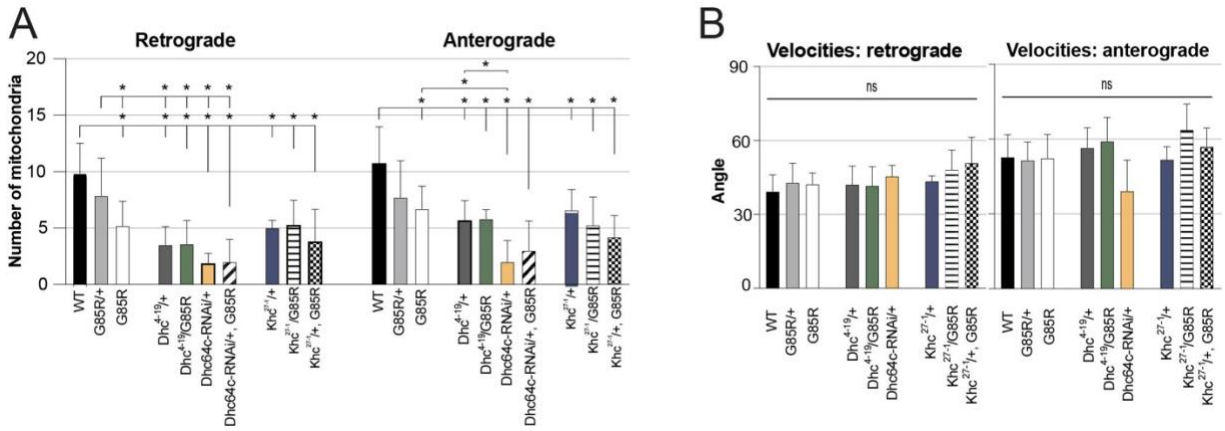

Supp 3: Defects in mitochondrial transport associated with loss of microtubule motors not enhanced in *dSod1*^{G85R}. **(A)** Quantification of number of mitochondria (mito-GFP) observed by live imaging moving in a retrograde or anterograde direction along MD axon in different genotypes: WT (n=19), G85R/+ (n=7), G85R (n=20), Dhc$^{4\text{-}19}$ /+ (n=6), Dhc$^{4\text{-}19}$ /G85R (n=5), Dhc64c-RNAi/+ (n=7), Dhc64c-RNAi/+, G85R (n=3), Khc$^{27\text{-}1}$ /+ (n=6), Khc$^{4/19}$ /G85R (n=4), Khc$^{4/19}$ /+, G85R (n=5); (**B)** velocity of mito-GFP movement in retrograde and anterograde direction was quantified from kymographs. Ordinary one-way ANOVA with Tukey's multiple comparison test, (*) p-value <0.05. Full genotypes in Table 1.

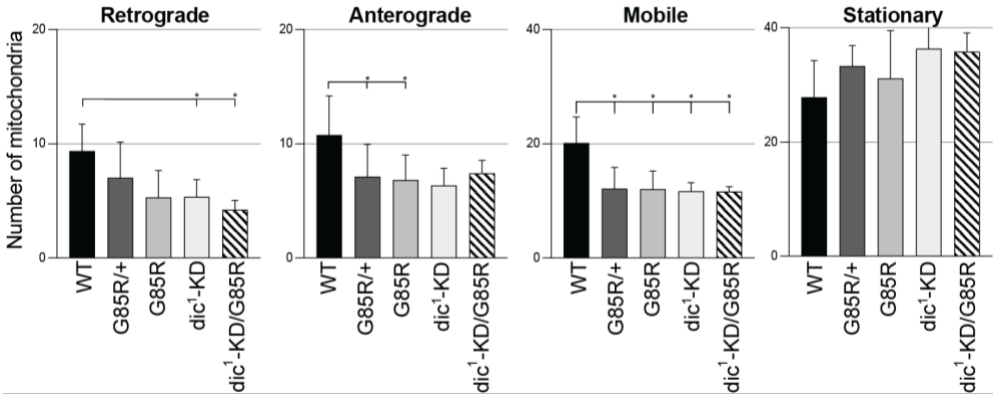

Supp 4: Dynein intermediate chain null allele, *dic[1]*, does not genetically interact with *dSod1[G85R]*. Retrograde, anterograde, mobile, and stationary mitochondria number, quantified from kymographs. **WT** (*w; MD-Gal4/+; UAS-mitoGFP + /+ dSod1[WT])* (n=17), **G85R/+** (*w; MD-Gal4/+; + /UAS-mitoGFP dSod1[G85R])* (n=10), **G85R** (*w; MD-Gal4/+; + dSod1[G85R]/UAS-mitoGFP dSod1[G85R]+*) (n=17), **dic[1]-KD** (*w; MD-Gal4/+; + dic[1]/UAS-mitoGFP dSod[WT] +*) (n=3), **dic[1]-KD/G85R** *(w; MD-Gal4/+; + dic[1]/UAS-mitoGFP dSod1[G85R]+*) (n=5). Ordinary one-way ANOVA with Tukey's multiple comparison test; (*) p-value <0.05.

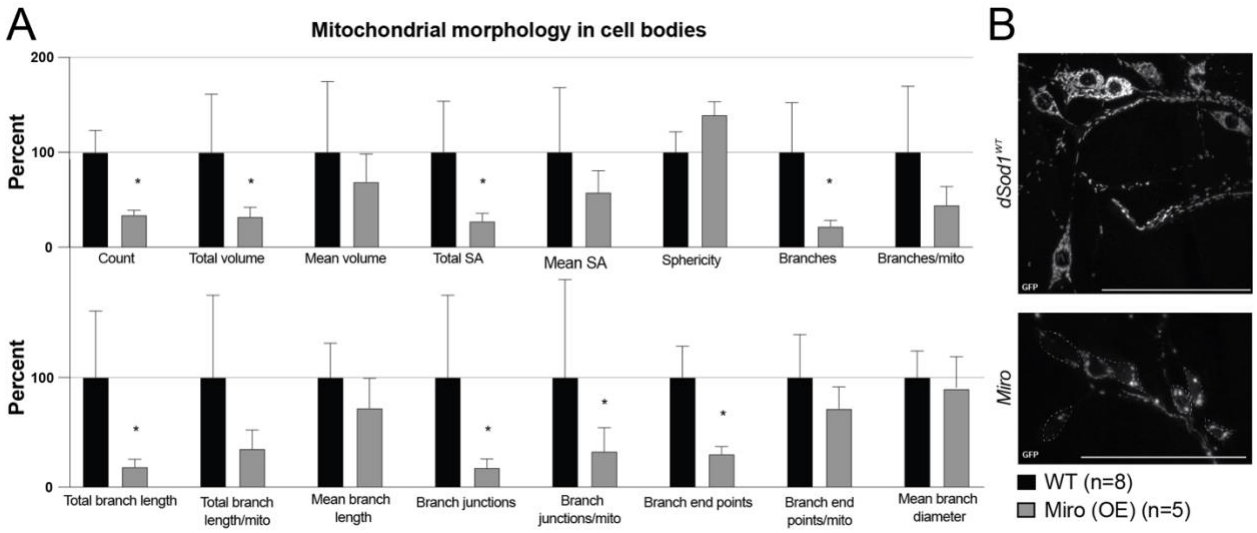

Supp 5: Overexpression of *Miro* alters mitochondrial morphology in MD neuron cell bodies. **(A)** Different structural parameters quantified using Mitochondria-Analyzer. **(B)** Confocal image of mito-GFP in WT (B-top) and Miro (OE) (B-bottom). *MD-Gal4/+;UAS-mito-GFP,dSod1^{WT}/+ (*or *UAS-Miro)*. Scale bar is 50um, student's t-test; (*) p-value <0.05.

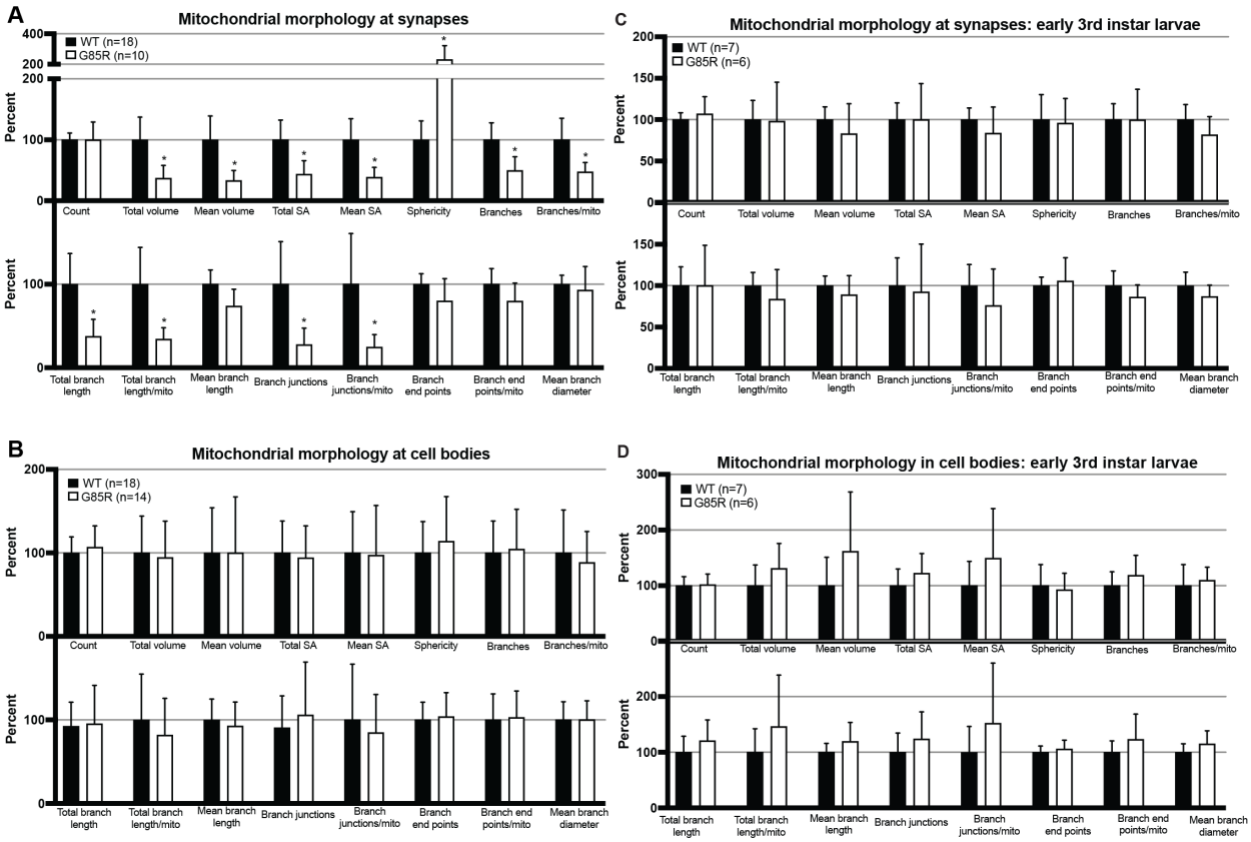

Supp 6: Mitochondrial morphology altered in *dSod1*^{G85R} MD synapses – full data set for Figure 3. **(A,B)** Quantitative assessment of mitochondrial morphology in synapses and cell bodies of WT (black bars) and G85R (white bars) wandering third instar larvae. **(C,D)** Quantitative assessment of mitochondrial morphology in WT vs G85R MD synapses (top) and cell bodies (bottom) in early third instar larval Student's t-test, (*) p-value<0.05.

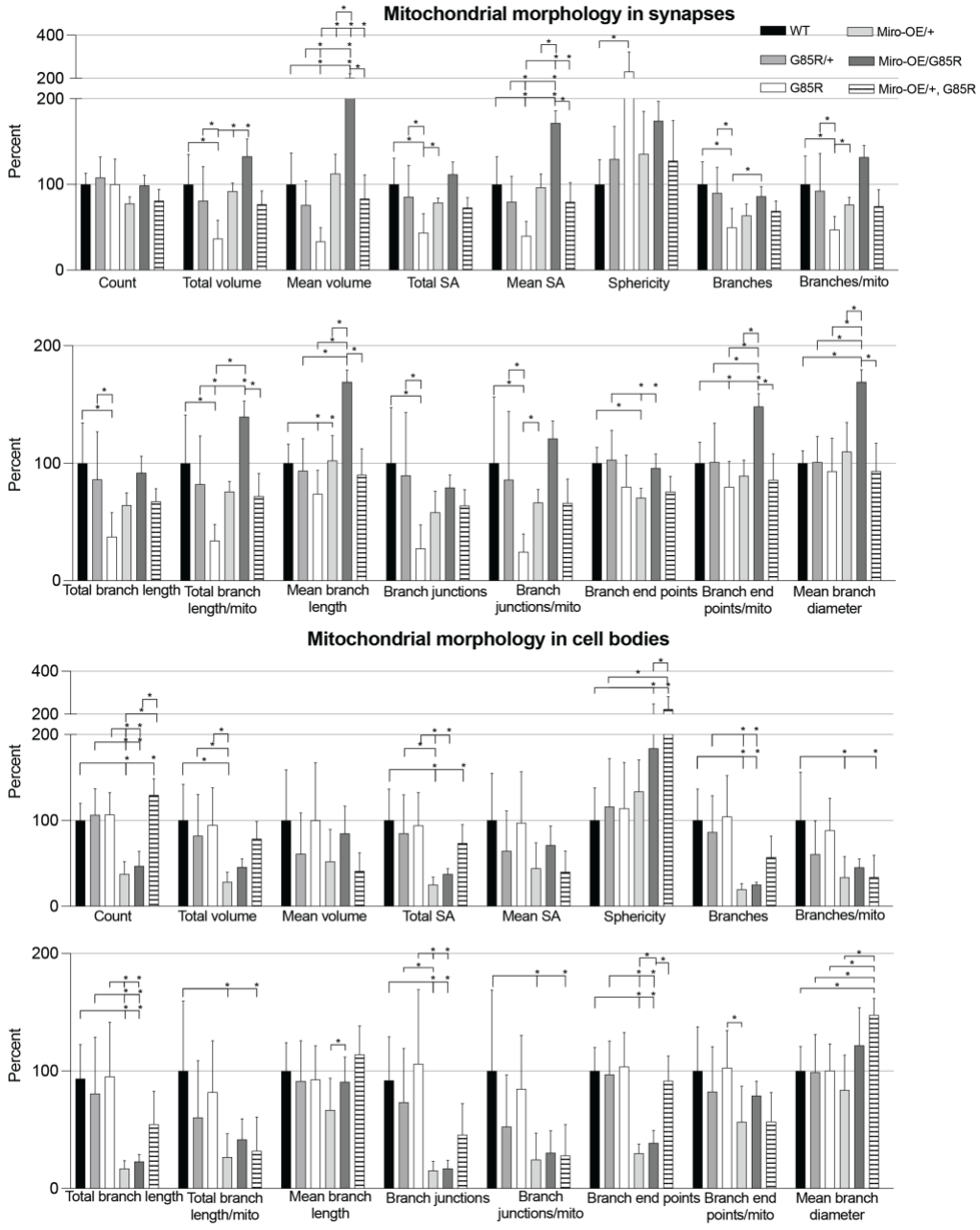

Supp 7: Overexpression of *Miro* (Miro-OE) rescues defects in mitochondrial morphology in MD neurons observed in *dSod1*^{G85R} homozygotes. Modified mitochondrial morphology observed when Miro-OE in *dSod1*^{G85R}/+ heterozygotes indicates a genetic interaction. Full dataset for Figure 5. Quantifications of different morphological parameters in synapses (top two panels) and in cell bodies (bottom two panels). WT (n=21), G85R/+ (n=15), G85R (n=8), Miro-OE (n=7), Miro-OE/G85R (n=4), Miro-OE/+, G85R (n=6), see Table 1 for full genotypes. Ordinary one-way ANOVA with Tukey's multiple comparison test; (*) p-value <0.05.

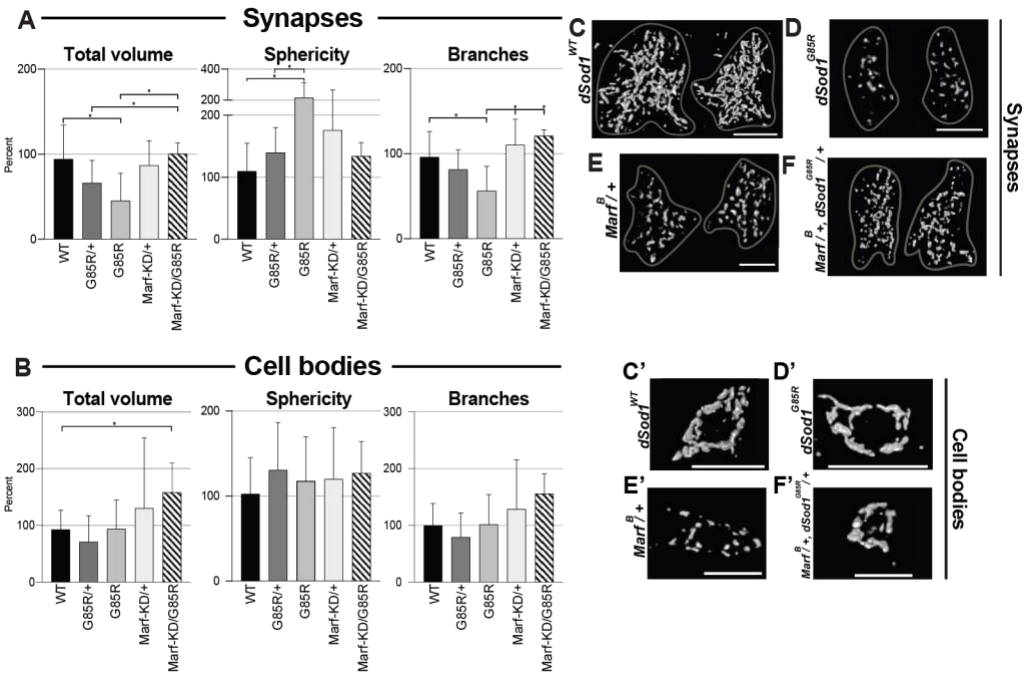

Supp 8: *Marf* knockdown does not rescue mitochondrial morphology defects in *dSod1*^{G85R} MD neurons. Quantifications of mitochondrial total volume, sphericity, and branches in MD neurons of *dSod1*^{G85R} larvae in relation to the functional null fission factor Marf, *Marf*^{B} (Marf-KD) **(A,B)**. Mitochondrial morphological changes in synapses **(A)** of WT (n=20), G85R/+ (n=16), G85R (n=17), Marf-KD/+ (n=3), and Marf-KD/G85R (n=3) 3rd instar larva, and cell bodies **(B)** of WT (n=20), G85R/+ (n=15), G85R (n=15), Marf-KD/+ (n=3), and Marf-KD/G85R (n=3) (Table 1 for full genotypes) 3rd instar larva. **(C-F)** 3D reconstruction of synaptic mitochondria at segments A2 of the VNC, left and right side, **(C'-F')** 3D reconstruction of mitochondrial at cell bodies of ddaE cell in the *da* cluster. Ordinary one-way ANOVA with Tukey's multiple comparison test; (*) p-value <0.05. All data from Mitochondrial Analyzer plugin in Supp 7.

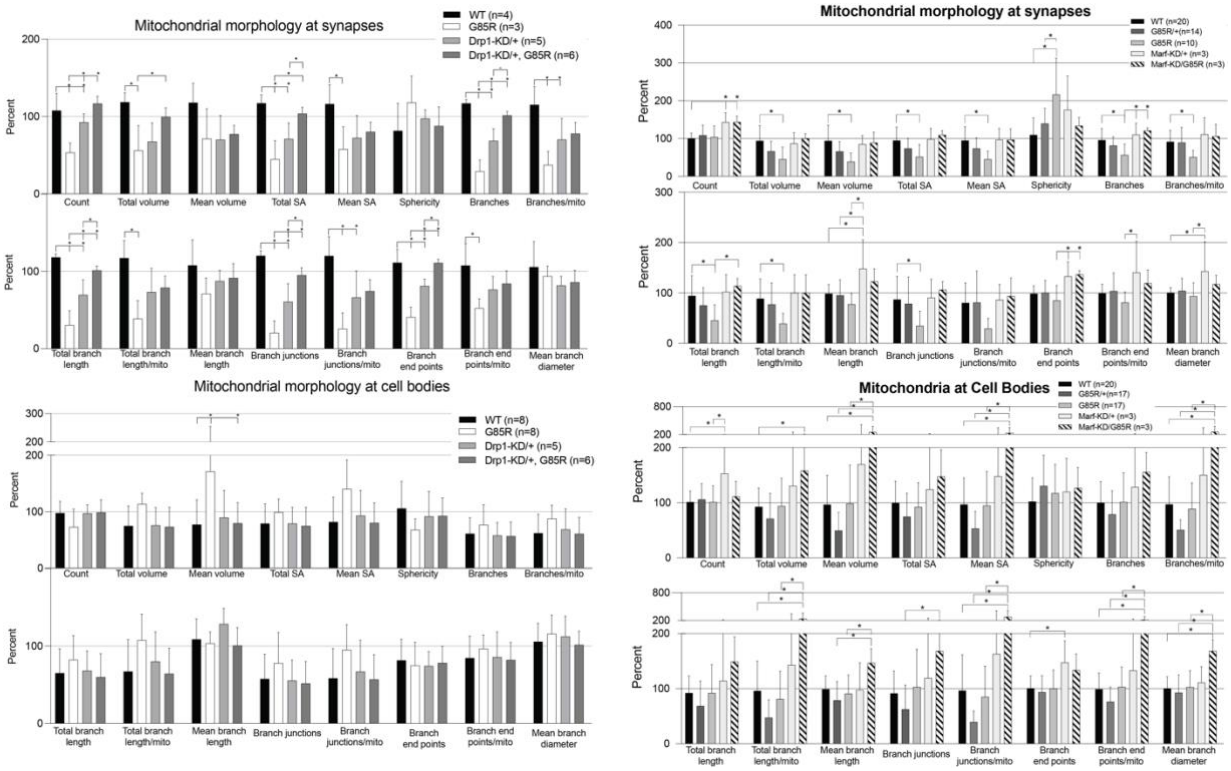

Supp 9: *Drp1* knockdown rescues mitochondrial morphology defects in *dSod1^{G85R}* MD axons, while Marf knockdown does not - full data sets for Figure 6, showing mitochondrial morphology outputs with manipulations of Drp1-KD and Marf-KD in MD neurons. Statistical analysis: one-way ANOVA with Tukey's multiple comparison test on normally distributed data, Kruskal-Wallis test with a Dunn correction for multiple comparisons on non-normally distributed data, (*) p-value <0.05.

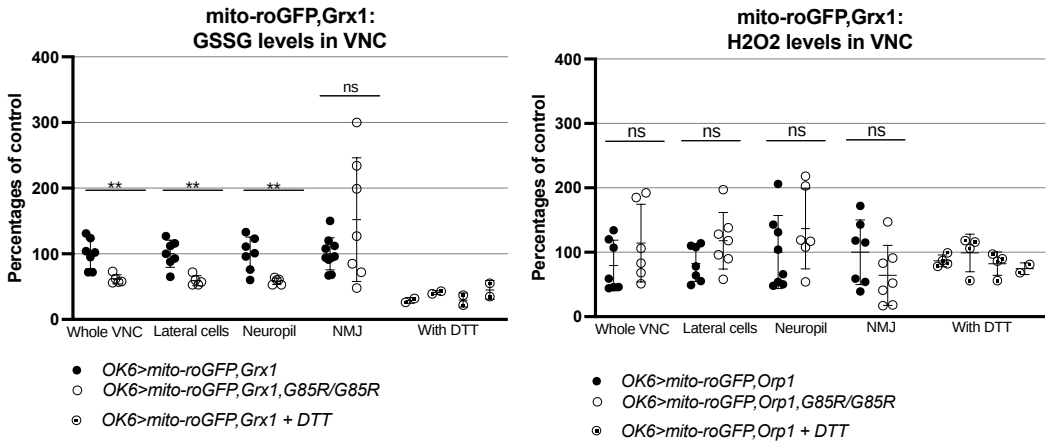

Supp 10: Decreased levels of mitochondrial glutathione redox couple in VNCs of *dSod1^{G85R}* motor neurons. Quantification of redox couples in *OK6-Gal4* motor neuron driver in whole VNC, lateral cells of the VNC, neuropil of the VNC, and the NMJ. VNCs treated with DTT reductant used as a positive control shows effectiveness of biosensor. Students' t-test, (*) p-value <0.05.

A

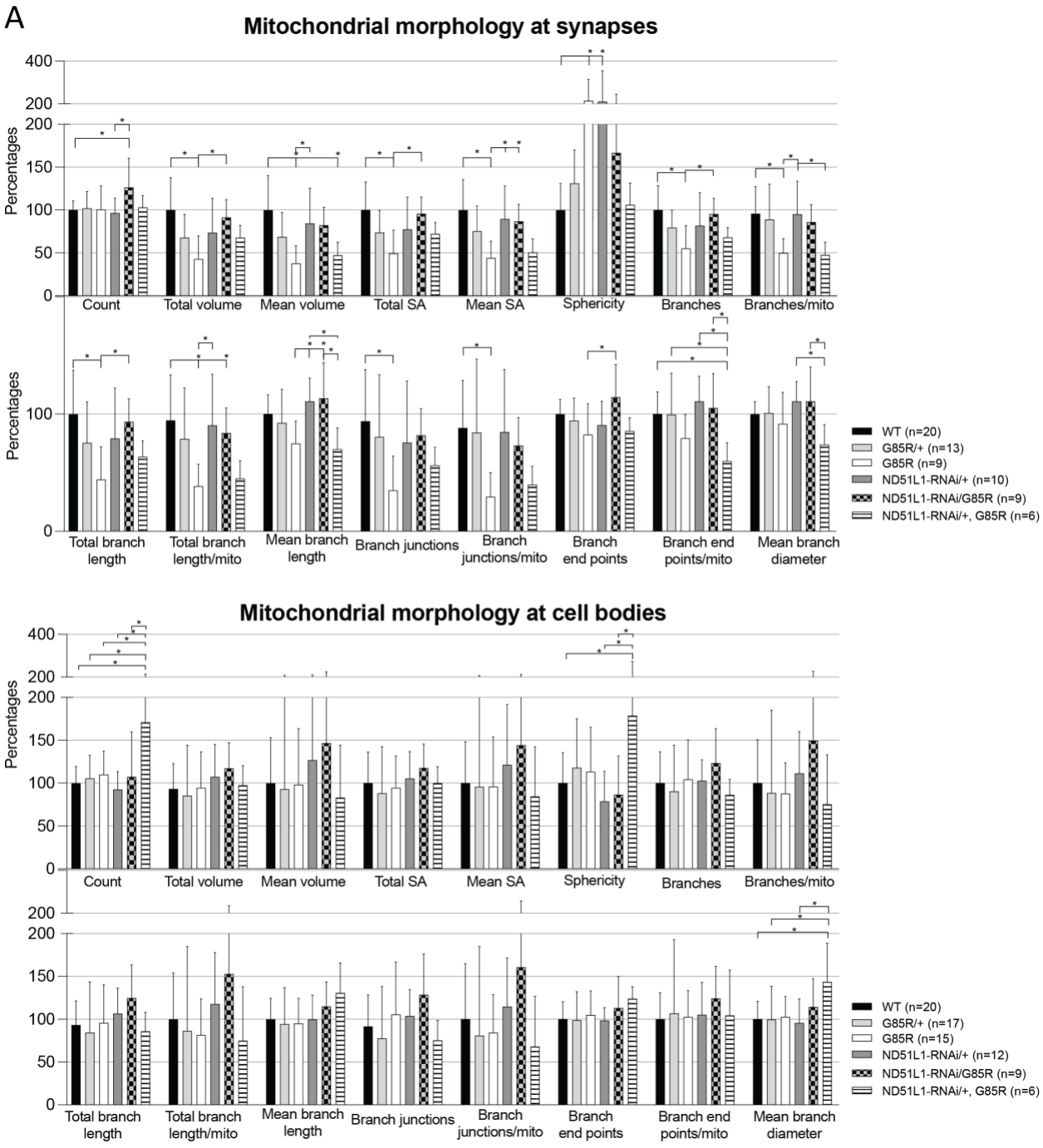

Supp 11A. Full legend below.

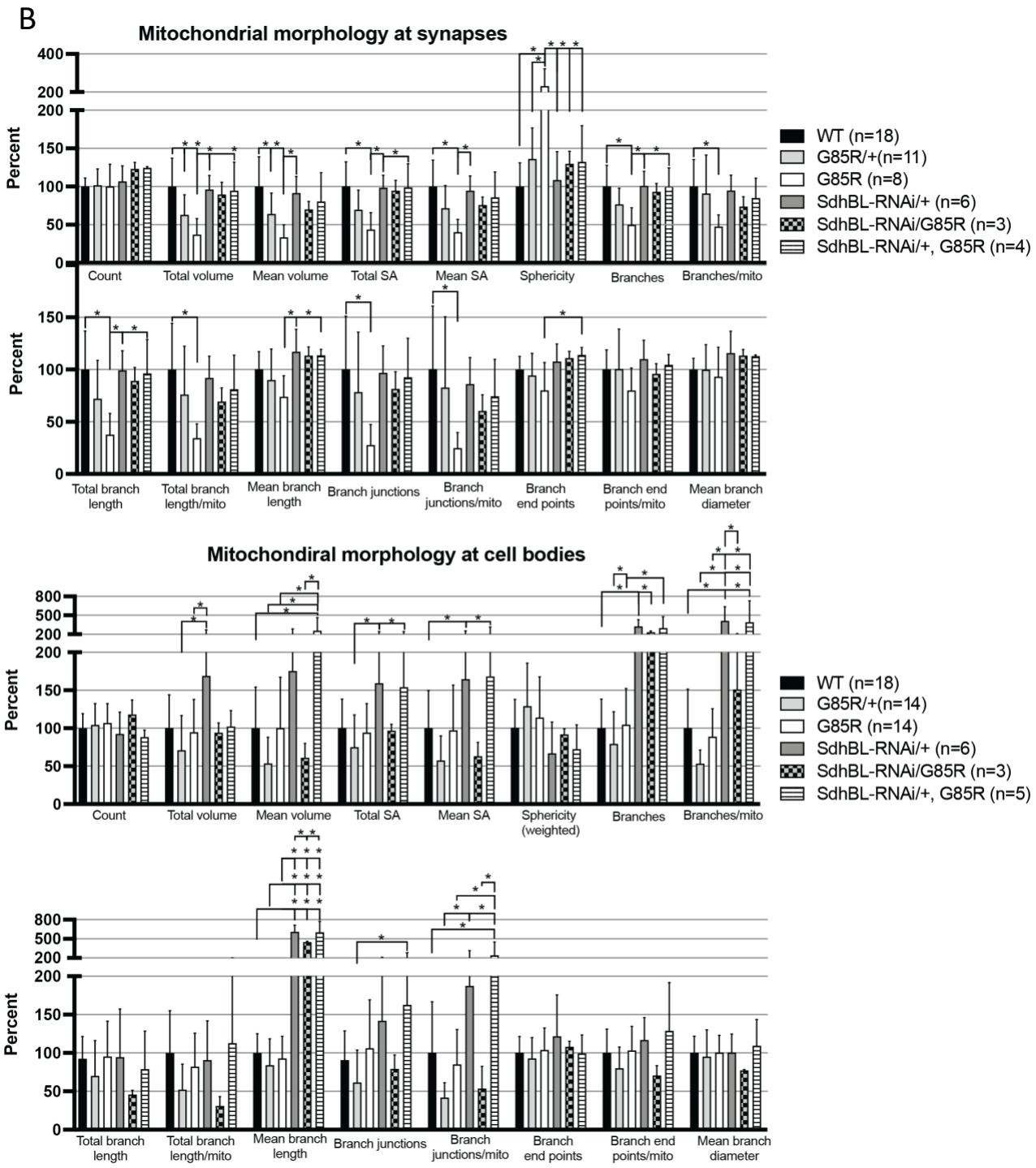

Supp 11B. Full legend below.

C

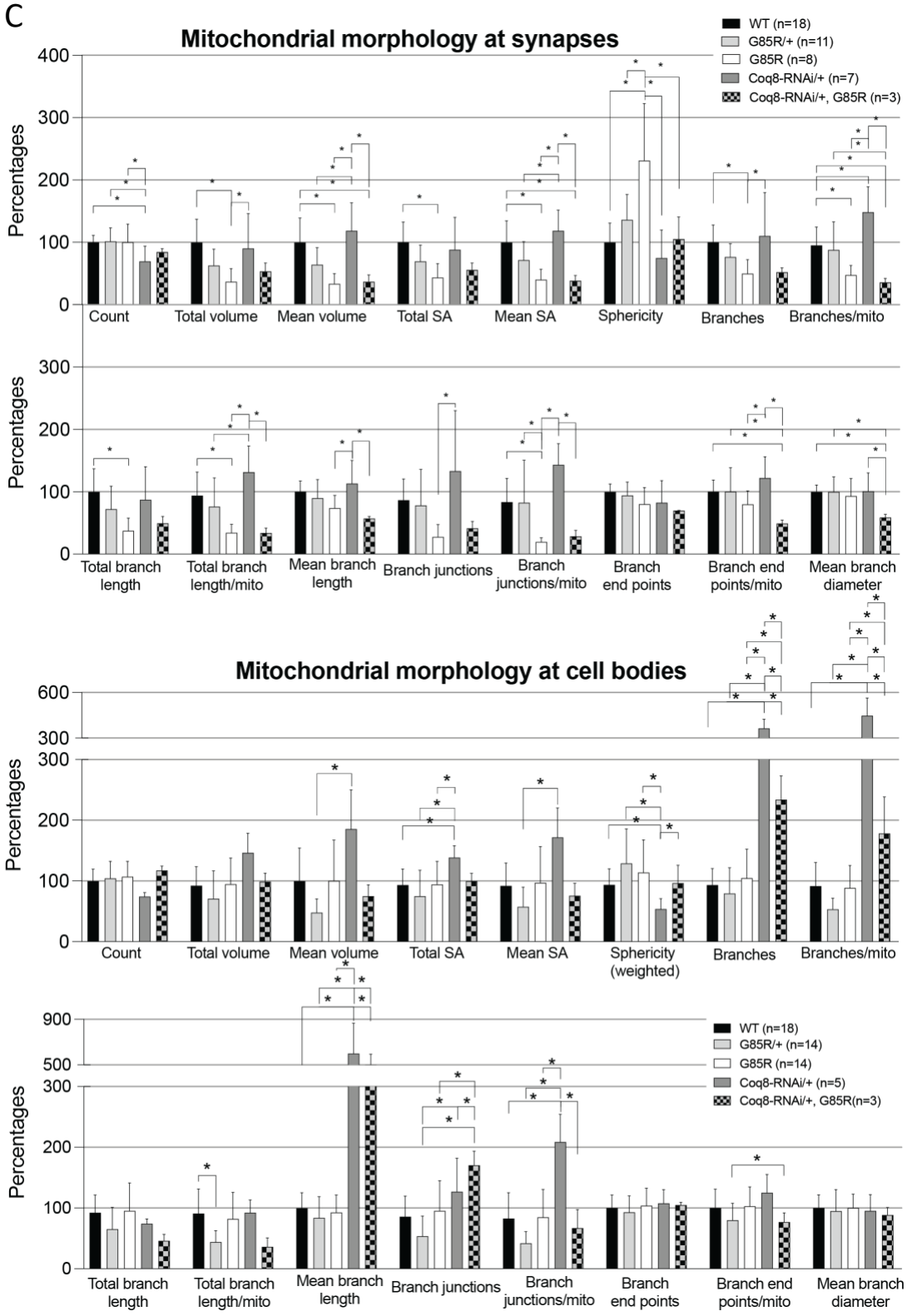

Supp 11C. Full legend below.

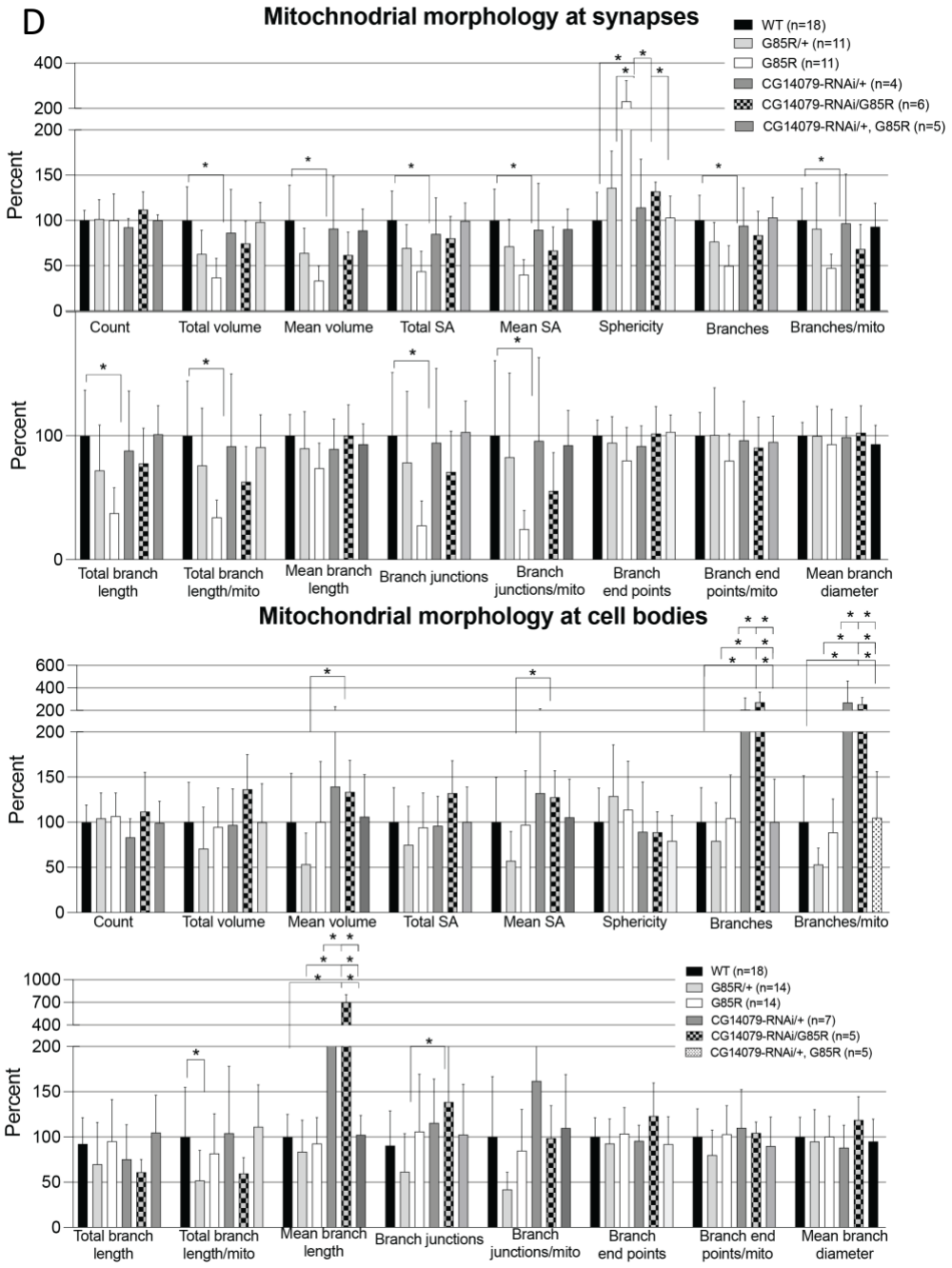

Supp 11: Knockdown of complex I, II, and IV subunits ameliorates mitochondrial morphological defects in *dSod1*^{G85R} MD neurons - full data sets for Figure 9, showing mitochondrial morphology outputs with manipulations of **(A)** ND51L1-RNAi, **(B)** SdhBL-RNAi, **(C)** Coq8-RNAi, and **(D)** CG14077-RNAi in MD synapses (top) and cell bodies (bottom). Table 1 for full genotypes. One-way ANOVA with Tukey's multiple comparison test on normally distributed data; Kruskal-Wallis test with a Dunn correction for multiple comparisons on non-normally distributed data, (*) p-value <0.05.

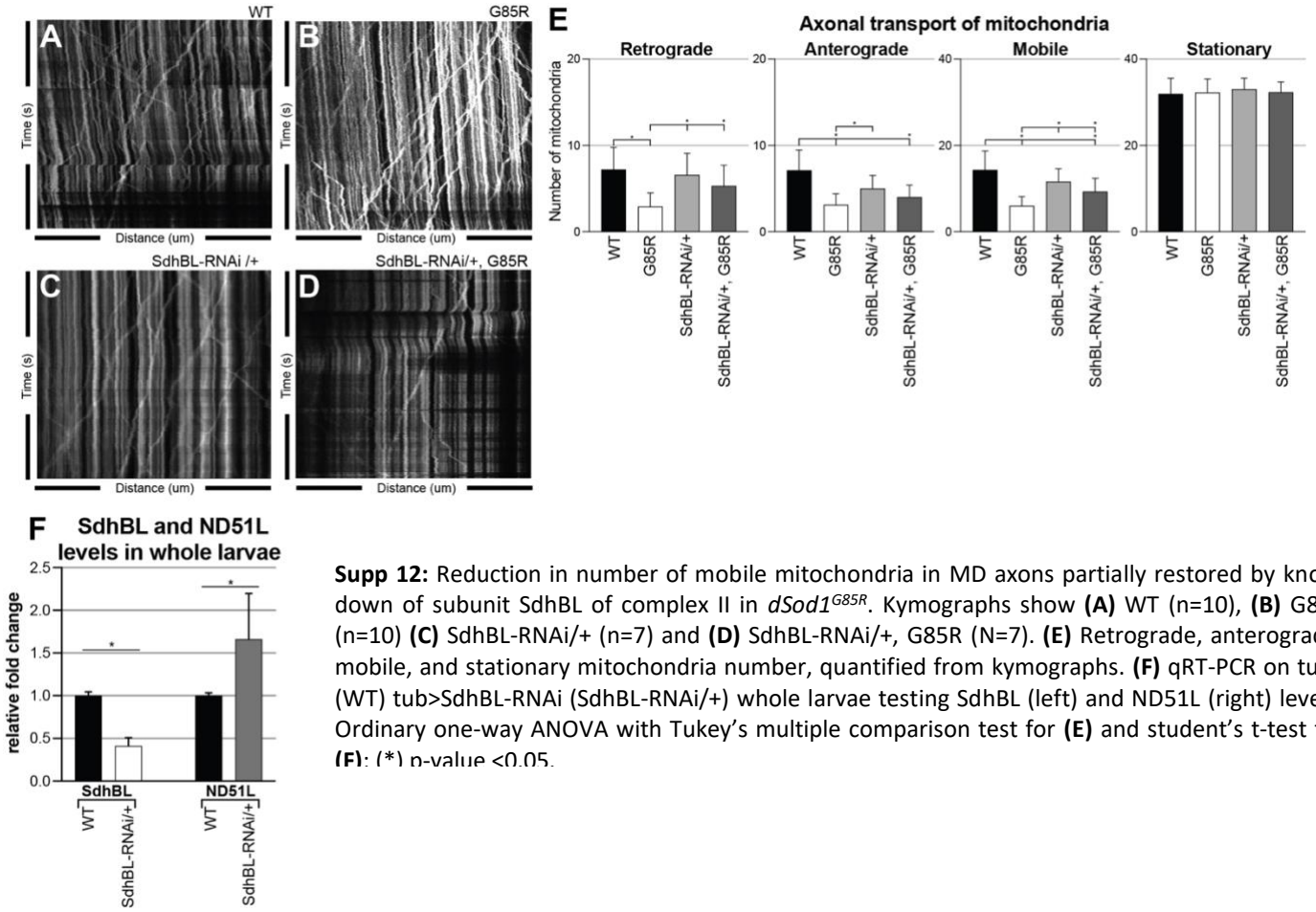

Supp 12: Reduction in number of mobile mitochondria in MD axons partially restored by knock down of subunit SdhBL of complex II in *dSod1^{G85R}*. Kymographs show **(A)** WT (n=10), **(B)** G85R (n=10) **(C)** SdhBL-RNAi/+ (n=7) and **(D)** SdhBL-RNAi/+, G85R (N=7). **(E)** Retrograde, anterograde, mobile, and stationary mitochondria number, quantified from kymographs. **(F)** qRT-PCR on tub> (WT) tub>SdhBL-RNAi (SdhBL-RNAi/+) whole larvae testing SdhBL (left) and ND51L (right) levels. Ordinary one-way ANOVA with Tukey's multiple comparison test for **(E)** and student's t-test for **(F)**; (*) p-value <0.05.